ELECTRICAL ENGINEERING
UNIVERSITY of WASHINGTON

BESS OPERATION USING VOLTTRON MULTI-AGENT PLATFORM

Deliverable UW9 of the project:
"Transactive Campus Energy Systems: An R&D Testbed for Renewables Integration, Energy and Grid Services"

Rémy Rigo-Mariani
Tu. A. Nguyen
Miguel Ortega-Vazquez
Daniel Kirschen

August 2016

Table of Contents:

ABSTRACT

Developed by the Pacific Northwest National Laboratory (PNNL) VOLTTRON is a multi-agent execution platform dedicated to power systems. This open source and modular software supports the communication between different entities over the grid. This report describes one example of agent development and software interactions for power management in a campus distribution grid. The experiment consists in optimizing the operation of an energy storage system based on a lithium-ion battery. An optimization is performed using a rolling window with a periodic refreshment of the forecasts for both production and consumption. The objective is to minimize the electrical bill while reducing the peak power and responding to transactive signals.

ACKNOWLEDGMENTS

The work presented in this report was carried out as part of the Clean Energy and Transactive Campus project in partnership with the Pacific Northwest National Laboratory (PNNL) and Washington State University (WSU). This project was supported by both the U.S. Department of Energy and the Washington State Department of Commerce Clean Energy Fund. The authors would like to thank PNNL for providing valuable advices regarding the VOLTTRON installation and deployment.

ACRONYMS

MAS	:	Multi-Agent System
JADE	:	Java Agent Development Environment
BESS	:	Battery Energy Storage System
MPC	:	Model Predictive Control
GAMS	:	General Algebraic Modeling System
API	:	Application Programming Interface
MPPT	:	Maximum Power Point Tracking
kNN	:	k-Nearest Neighbor
TS	:	Transactive Signal

LIST OF SYMBOLS

$T_{refresh}$	:	Refreshment period between optimization	min
P_{PV}	:	Photovoltaic production	kW
P_{load}	:	Consumption	kW
P^{P}_{PV}	:	Production forecast	kW
P^{P}_{load}	:	Consumption forecast	kW
G	:	Solar radiation	W/m^2
G_{clean}	:	Clean sky solar radiation	W/m^2
G^{P}	:	Predicted solar radiation	W/m^2
T	:	Outdoor temperature	^{o}F
T^{P}	:	Predicted outdoor temperature	^{o}F
$\tau_{refresh}$	:	Refreshing period	min
τ_{pred}	:	Prediction horizon	min
τ_{lag}	:	Screened past time to perform the forecast	min
CC	:	Cloud cover	%
λ	:	Energy rates	$/kWh
λ_{peak}	:	Cost of peak demand	S/kW
λ_{TS}	:	Transactive price-like signal	S/kWh
P_{bat}^{+}	:	Charge power of the BESS	kW
P_{bat}^{-}	:	Discharge power of the BESS	kW
SOC	:	State of charge	%
E_{bat_max}	:	Maximum energy stored in the battery	kWh
V_{bat}	:	Battery voltage	V
I_{bat}	:	Battery current	A
N_{para}	:	Number of cells in parallel	-
N_{serie}	:	Number of cells in series	-
$\eta_{bat}^{+}, \eta_{bat}^{-}$	:	Battery efficiency in the linear model	%
η_{cvs}	:	Converters efficiency	%

1 INTRODUCTION

Multi-Agent Systems (MAS) had received extensive interest to enhance the control of complex distributed power systems [Kantamneni 15]. In a multi-agent framework the intelligence is distributed with each entity acting independently in order to satisfy a global objective. One of the main advantages of MAS is its scalability and fulfillment of privacy constraints with a limited number of information exchanged between the participants. Many examples of MAS for power systems control can be found in the literature from the large-scale utility side with voltage regulation [Zhang 16] to the management of buildings in Demand Response environments [Labeodan 15]. Open sources platforms for agent development exist for the past two decades and allows implementing control methods for smart grid. In particular the JADE (Java Agent Development Environment) and ZEUS are Java based platform that allows deploying agent using GUI interface and providing run time environment or tools for combining Matlab/Simulink [Kantamneni 15]. VOLTTRON is a command line Python based platform developed by the Pacific Northwest National Laboratory (PNNL) dedicated to the management of entities over the electrical grid [Haack 13]. Communications are established thought a central message bus and the platform offers many functionalities such as Modbus/Bacnet driver or SQL database for data acquisition. Most the published current applications using VOLTTRON platform refers to building management with sensors and load scheduling [Khamphanchai 14] or model predictive control for heating and air conditioning system [Hao 16]. However the flexibility and scalability of the platform make it promising for management strategy involving different type of electrical equipment. This report presents an agent deployment for the optimal management of a battery energy storage system (BESS) with PV panels in a campus distribution grid at the University of Washington, Seattle. The document is organized as follow:

- Section 2 describes the strategy chosen to run the system with the agent organization
- Section 3 details the implementation of the agents
- Section 4 give some simulations results

2 AGENT ARCHITECTURE

2.1 BESS Operation

The University of Washington aims at purchasing a total capacity of 100 kW of PV panels settled on three of his dorms in addition to a Li-Ion Battery of 325 kWh that would be installed in the basement of the Electrical Engineering building. The management of the BESS relies on an optimal scheduling performed on a rolling windows basis of 24 h with a refreshment every $T_{refresh}$ (30 min by default here) (Fig.1). Every time the optimization is performed the forecast for the production, the consumption and the energy prices are refreshed. Also the state of charge (*SOC*) of the battery is actualized based on measurements in order to fulfill the overcharge/overdischarge constraints in the process. The optimization is based on a cost minimization with arbitrage between day and night prices as well as peak power control. The system should also be able to answer to unpredicted transactive signal (TS) that are likely to occur during its operation. Those transactive signal will be considered as price-like values and would aim at encouraging an increase or decrease of the net load depending on the needs of the grid. That aspect is part of the Transactive Framework that aims at enhancing the efficiency of the power grid with a multi-agents that interact based on bid-auctions mechanisms which is not in the scope of the presented work.

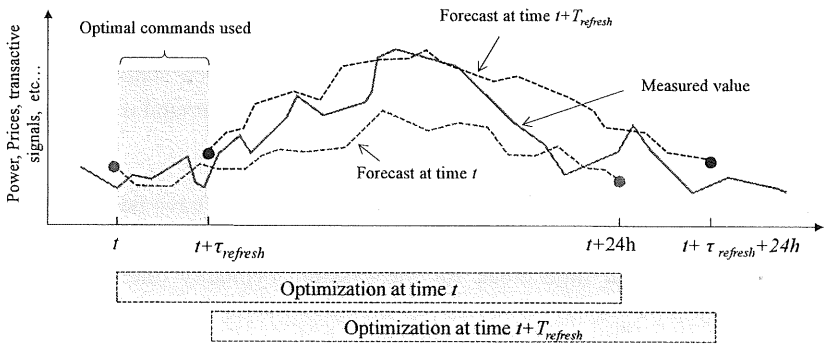

Fig.1: Rolling window optimization

2.2 Multi-Agent deployment

Volttron offers a Python development environment to implement the agents using object oriented programming. Especially those agents exchange information though a common message bus on a publish/subscribe basis. The python environment allows the communication with a wide range of external softwares (Matlab, GAMS, SQL servers,....) with dedicated Application Programming Interfaces (APIs) Fig.2 displays the proposed Volttron architecture to implement the proposed management strategy:

1. Both consumption and production continuously publish their measured values on the message. At every time step the data are stored in the platform historian on a SQL database.

2. At every $T_{refresh}$ a central management agent send queries that trigger the forecasts for the load, PV and prices profiles.

3. Especially as it will be developed in the next section the forecasts for the consumption/production require to access to the last measured values stored in the historian.

4. An optimization agent then gathers all the predictions as well as the current *SOC* for the battery before computing the scheduling for the BESS operation using GAMS (General Algebraic Modeling System).

5. The optimal controls are finally sent to the battery controller.

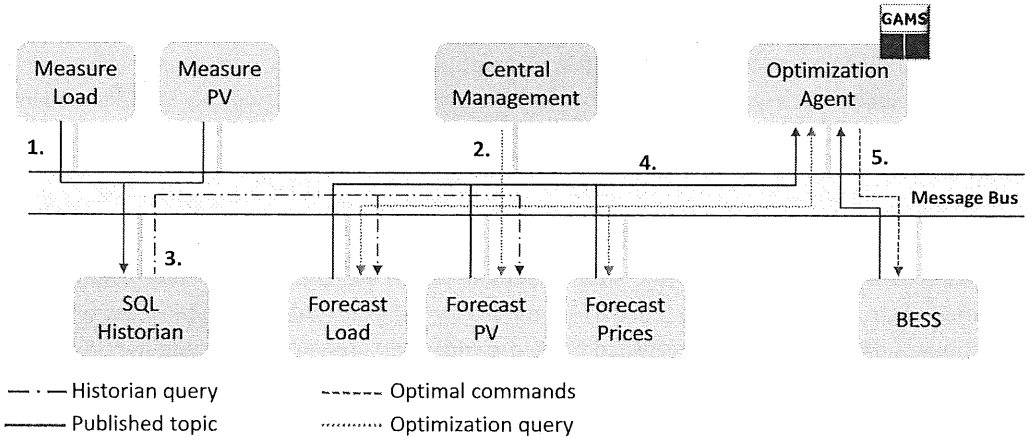

Fig.2: Proposed Volttron architecture

Note that the approach refers to a model predictive control (MPC) of the BESS with a simplified model of the battery implemented in GAMS. Thus the local battery controller would have to deal with the actual measurements that do not necessary comply with the predicted schedule in order to fulfill the operation constraints. That local controller considers the scheduled command until they are refreshed when a new optimization is performed with actualized inputs.

Note that at the moment nor PV modules and nor smart meters have been installed yet on the UW campus. Thus the real time simulation of the proposed architecture using the Volttron platform need an additional agent that fake a real time clock for the system. Typically one second simulation will be equivalent to 1 minute.

3 AGENT IMPLEMENTATION

3.1 Measure Load and PV

Load P_{load} and PV production P_{PV} are emulated using measurements on site. A whole year (October 2014 to October 2015) of data is available with a time step of 15 min for the Electrical Engineering and Computer Science Building. The profile show significant base load around 850 kW with peaks around 1000 kW with maximums values of 1200 kW for a total yearly consumption of 8.3 GWh. Another set of measurement is performed the two last weeks of September 2016 with a time resolution of 5 min. Those data will be used in the following simulations and displays strong correlation of the load from one day to the other with similar profiles (Fig.3).

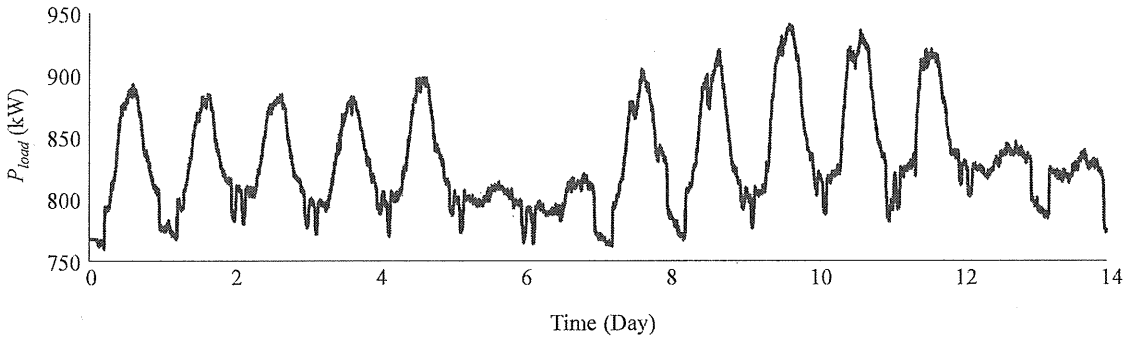

Fig.3: Two weeks load profile (September 2016)

For the production another set of measurements is performed from January 2016 to October 2016 using the real time values of the weather stations belonging to Weather Underground. An agent in Volltron uses the Weather Underground API (http://www.wunderground.com/weather/api/) to retrieve, among other, the solar radiation G (in W/m^2) and the outdoor temperature T (in ^{O}C). The measurements are performed every 5 min considering the weather station labelled "KWASEATT446" (the closest station with solar radiation meter) and profiles are saved in one .csv file per month. Recorded data have to be repaired in order to correct the missing points or extreme values. Fig.4 displays sample results for successive days of September 2016. In particular the solar radiation values are compared to the profiles returned by a simplified clean sky model G_{clean} [Bird 81] provided by the National Renewable Energy Laboratory and that estimates direct, diffuse and reflected beam depending on pressure, ozone and humidity conditions.

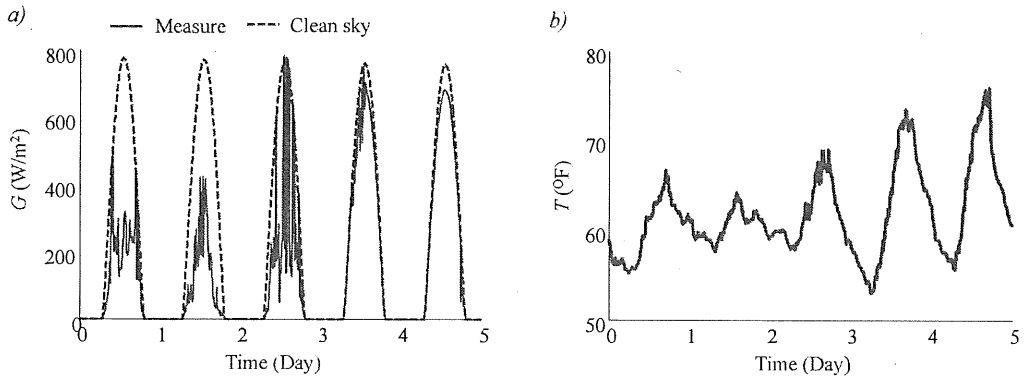

Fig.4: Weather data - a) solar radiation - b) temperature

The measured weather conditions are then send to the PV system model described by and referring to a simple single diode models for the modules [Darras 10] assuming that the MPPT (Maximum Power Point Tracking) is correctly achieved. Especially the model requires information provided by the array manufacturer (Intek 280 W arrays here, http://www.itekenergy.com). A total number of 359 modules are considered for an installed capacity of 100 kW dispatched on three dorms buildings in the UW campus (see Appendix A for more details). Note that the temperature data has to be converted from Fahrenheit to Celsius.

$$P_{PV} = \eta_{cvs} \times N_{PV} \times \frac{G}{G_R} \times \left(P_{PV\_max} + \mu_{P\max} \times \left(T_j - T_{jR}\right)\right) \text{ with } T_j = T + G \times \frac{NOCT - 20}{800} \quad \textbf{Eq.1}$$

With:

- P_{PV} : power produced by the array (in kW)
- N_{PV} :number of array in the considered PV system ()
- G_R : solar radiation in standards conditions (= 1000 W/m²)
- $P_{PV\_\max}$: maximum output power of a single array (in kW)
- μ_{Pmax} :the negative deviation of the output power with the temperature (in %./°C)
- T_j : the junction temperature of the modules (in °C)
- Tj_R : the junction temperature in standards conditions (= 25°C)
- $NOCT$: the nominal operation cell temperature (in °C)
- η_{cvs} : constant converter efficiency (typically 95 %)

The implemented model also takes account of the parameters of the photovoltaic installation in terms of tilt θ_t and orientation θ_o both in degrees. The approach requires computing the solar position (elevation α_e and azimuth angles α_a) depending on the considered day in the year and global position. Then Eq.2 is used in order to correct the solar radiation on the collector by computing the angle of incidence β (Eq.3) [Masters 13]. Based on the preliminary design, the installation is set with a tilt at 10.4 ^{O} and oriented South ($\theta_o = 0\ ^{O}$). Fig.5 displays the profiles obtained for two weeks in September 2016 based on measurement for solar radiation and temperature. See Appendix B for the detailed computation of the solar angles.

$$\cos\beta = \cos\alpha_e \times \cos\left(\theta_o - \alpha_a\right) \times \sin\theta_t + \sin\theta_t \sin\alpha_e \quad \textbf{Eq.2}$$

$$G \leftarrow G \times \cos\beta \quad \textbf{Eq.3}$$

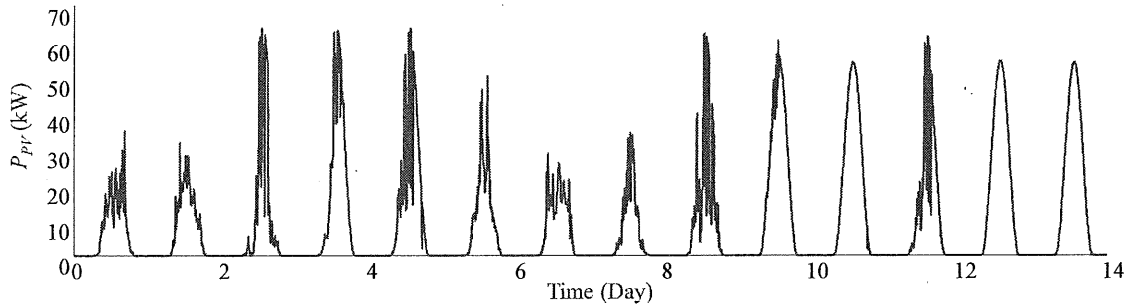

Fig.5: Two weeks PV production profile (September 2016)

3.2 Forecast Agents

3.2.1 Consumption Prediction

As explained in the previous section, at every $\tau_{refresh}$ an optimal scheduling for the storage controls is required and trigger the generation of new forecast for the consumption, the production and the prices. Regarding the consumption and based on the previous observations the prediction P^{P}_{load} is based on a simple persistent day to day model (t – 24 h). When the prediction is performed at time t the previous measured values are screened until $t - \tau_{lag}$ (with τ_{lag} in time steps). Then the values measured 24 h before are corrected following Eq.4 in order to generate the forecast from t to t + 24 h (receding horizon of 24 h considered here). That correction is based on an offset of the 24 h value depending on the measured mean deviation for the past time steps.

$$P^{P}_{load}(t) = P_{load}(t-24\,\text{h}) + \frac{1}{\tau_{lag}} \times \left(\sum_{p=1}^{\tau_{lag}} P_{load}(t-p) - P_{load}(t-p-24\,\text{h}) \right) \qquad \textbf{Eq.4}$$

Fig.6 shows the forecasted versus the measured values for a week day of September with prediction successively performed at 8:00, 13:00 and 18:00 with τ_{lag} = 60 min Note that if the prediction horizon is 24 h long only the forecasted value until the end of the considered day are displayed here. The profiles show that the prediction is accurate for the consecutive time steps and the deviation tends to increase with longer hirizon. Also the offset correction proves itself efficient with a predicted peak value corrected when the forecast is performed at 13:00 (moving from Fig.6*a* to Fig.6*b*). The prediction for the end of the day is also improved when the forecast is refreshed at 18:00 ((moving from Fig.6*b* to Fig.6*c*)).

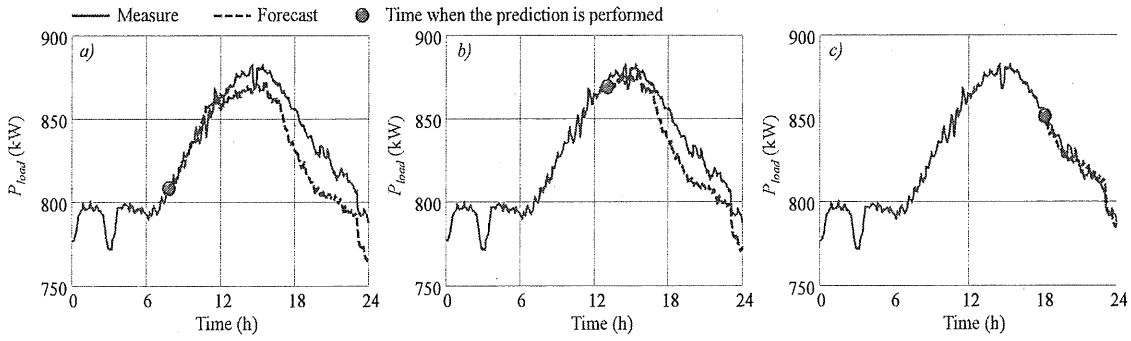

Fig.6: Sample of load forecast – *a)* at 8:00 – b) at 13:00 – *c)* at 18:00

Additional studies are made to estimate the prediction error with the proposed method. Random prediction samples (N_{sampl}=200) performed at different time are considered for the measurements of September 2016. In each case both root mean square error $\mathcal{E}_{RMS}$ and relative error $\mathcal{E}_R$ are computed using Eq.5 and Eq.6 for different prediction horizon τ_{pred} while considering the prediction and measurements samples ($P^P_{load,s}$ and $P_{load,s}$)

$$\varepsilon_{RMS}(\tau_{pred}) = \sqrt{\frac{1}{\tau_{pred} \times N_{sampl}} \times \sum_{s=1}^{N_{sampl}} \sum_{t=0}^{\tau_{pred}} \left(P^P_{load,s}(t) - P_{load,s}(t)\right)^2} \quad \textbf{Eq.5}$$

$$\varepsilon_R(\tau_{pred}) = \frac{1}{\tau_{pred} \times N_{sampl}} \times \sum_{s=1}^{N_{sampl}} \sum_{t=0}^{\tau_{pred}} \frac{\left|P^P_{load,s}(t) - P_{load,s}(t)\right|}{P_{load,s}(t)} \quad \textbf{Eq.6}$$

Fig.7 displays the result obtained when different values of τ_{lag} are investigated while performing the offset correction. It is worth noticing that correcting the previous day measurements strongly improved the quality of the prediction moving the RMSE from 23 kW down to around 5 kW when forecasting 5 min ahead (Fig.7*a*) compare to a case with no offset. With that corrected offset the prediction error tends to increase for longer prediction horizon and the observed values remains low with less than 1 % of relative error (Fig.7*b*). It is also noticeable that increasing the value of τ_{lag} slightly decreases the prediction performances. Thus in the simulations that will be performed in the next section, forecasts will be performed by considering τ_{lag} of 5 min (i.e. a single time step). Note that with no corrected offset the computed error is almost constant no matter the considered prediction horizon. That error corresponds to the deviations of the loadprofiles between successive days. The low value observed are partly explained by the similarity of the profiles but mostly by the significant base load that represent 90 % of the consumption when the peak occurs (Fig.2).

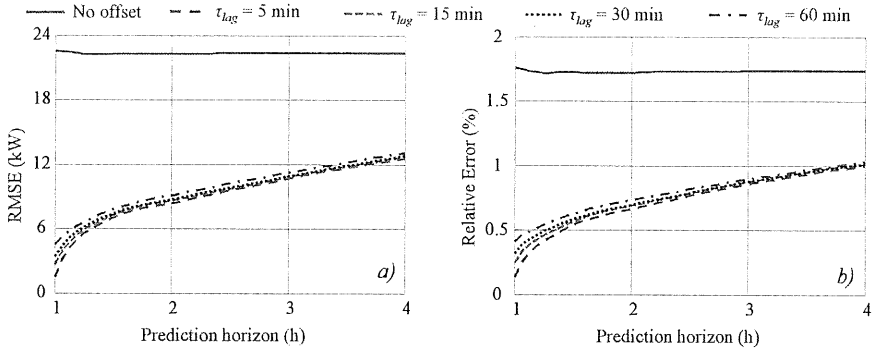

Fig.7: Prediction Error Vs Prediction horizon – *a)* RMSE – *b)* relative error

With such a chosen approach to generate the forecast based on previous day measurements the distinction has to be made between week days and the ween-ends as illustrated on Fig.8.

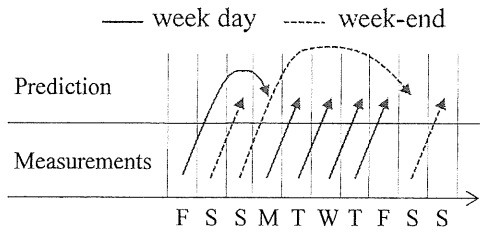

Fig.8: Previous day measurements for day ahead forecast

3.2.2 PV production Prediction

The solar forecasting methods are divided into two main classes, the statistical approaches on one hand and the numerical weather prediction models (NWP) on the other [Diagne 13]. The choice of a method is closely linked to the considered time horizon and the type of data available to perform the forecast (time sampling and space distribution). Indeed an intra hour forecast would be hazardous if only hourly based samples of data are available. Physical complex meteorological models are accurate for long term prediction from several hours to several days ahead while statistical approaches have good performances for intra hour forecast. In the present work the management strategy relies on a receding horizon optimization with refreshed forecast every $\tau_{refresh}$). The choice is made here to have a "hybrid" prediction using two distinct models to perform the forecast with different time resolutions. Indeed if the forecast in $[t\ ,\ t+\tau_{refresh}]$ needs a high resolution we cannot expect the model for the whole 24 h window to have the same time step.

3.2.2.1 Long Term Forecast

Solar radiation and outdoor temperature long term forecasts (G^P and T^P) are compute using the 24 h ahead prediction provided by Weather Underground. Those predictions are refreshed every hour and a returned with an hourly time step. Note that the solar radiation is not directly available in the extracted data. Instead the cloud cover CC is forecasted with values between 0 % and 100 %. Those estimations are corrected using Eq.7 in order to compute the predicted solar radiation G^P computing the clean sky profile G_{clean} for the corresponding date-time points [Perez 07]. The clean sky value are once again computed using the BIRD model.

$$G^P = G_{clean} \times \left(1 - 0.87 \times \left(\frac{CC}{100}\right)^{1.9}\right) \qquad \textbf{Eq.7}$$

3.2.2.2 Short Term Forecast

For the short term forecast (up to one hour ahead with a 5 min discretization) a statistical approach is considered. Among the possible methods Autoregressive Moving Average (ARMA) and Neural Networks (NN) are widely used in the literature [Diagne 13]. In the present work the choice is made to use the k-Nearest Neighbor (kNN), a very simple and "lazy" machine learning method based on pattern recognition for time series [Pedro 12]. Measured values of the variable X from $t - \tau_{lag}$ are used to compute the prediction X^P from t to $t + \tau_{pred}$ using N_{train} training samples $X_{tr,s}$. The distance $d(X, X_{tr,s})$ between the observed X and the every training profile is computed using Eq.8. Then the nearest neighbors profiles (NN) are selected and ranked in a descend order from X_{tr,NN_1} to X_{tr,NN_k} with k the number of considered NN. Finally the prediction is computed using Eq.9 with a weight average of the selected NN [Lora 02].

$$d(X, X_{tr,s}) = \sqrt{\sum_{p=1}^{\tau_{lag}} \left(X(t-p) - X_{tr,s}(t-p)\right)^2} \quad \text{for } s = 1 \ldots N_{train} \qquad \textbf{Eq.8}$$

$$X^P(t) = \frac{1}{\sum_{i=1}^{k} w_i} \times \sum_{i=1}^{k} w_i \times X_{tr,NN\_i}(t) \quad \text{for } t = 1 \ldots \tau_{pred} \quad \text{with} \quad w_i = \frac{d(X, X_{tr,NN\_k}) - d(X, X_{tr,NN\_i})}{d(X, X_{tr,NN\_k}) - d(X, X_{tr,NN\_1})} \qquad \textbf{Eq.9}$$

In the study the 5 min interval measurement collected between January 2016 and August 2016 are used as training samples. Then the profiles of September 2016 are considered to test the short term forecasts. Note that for the solar radiation, the predicted time series is the clarity index K_c compute as the ratio

G / G_{clean}. The idea is to removing the daily/seasonal effects correlated to the deterministic positon of the sun as in [Paoli 10]. Thus the measured data are pre-processed to extract training and test samples for the clarity index. Then when the short term forecast is performed the clarity prediction K_c^P is used to obtain the PV profile. In appendix C different simulations are run to test the short term predictor with different parameters of the kNN in order to find the best configuration. Finally the number of considered nearest neighbors is set to $k = 10$ and the τ_{lag} is set to 15 min (i.e 3 time steps here).

3.2.2.3 Obtained Results

The solar production prediction tool is finally implemented as detailed on Fig.9 with a hybrid predictor that considers hourly forecast for long term planning and past time step measurements to generate short term prediction with the kNN method. Note that the computation of the solar angles all along the prediction horizon is required to correct the power produced by the PV systems at each forecasted time step. Also the long term forecast are discretized with a time step of 5 min even if the values retrieved using Weather Underground are given on a hourly basis.

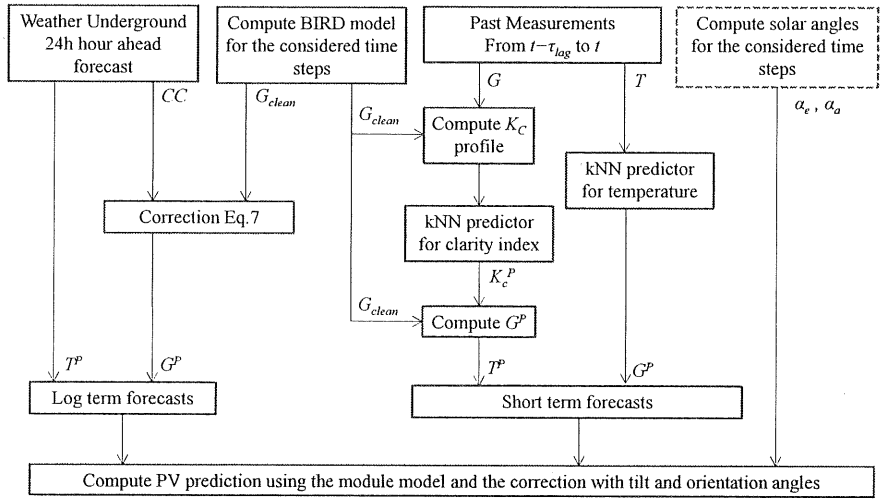

Fig.9: Forecast tool for the PV production

Fig.10 displays the results obtained for a tested day in September 2016 with successive predictions performed. When the forecast is performed at 8:00 (Fig.10*a*) the Weather Underground service returns close cloud cover values all along the day which explains the "clean" overall predicted profile. Small deviations can only been observed between 12:00 and 13:00 with different *CC* values. On (Fig.10*b*) the difference between short term forecast (1 h ahead here) can be observed with a more dynamic profile compared to the long term trajectory computed with the clean sky model.

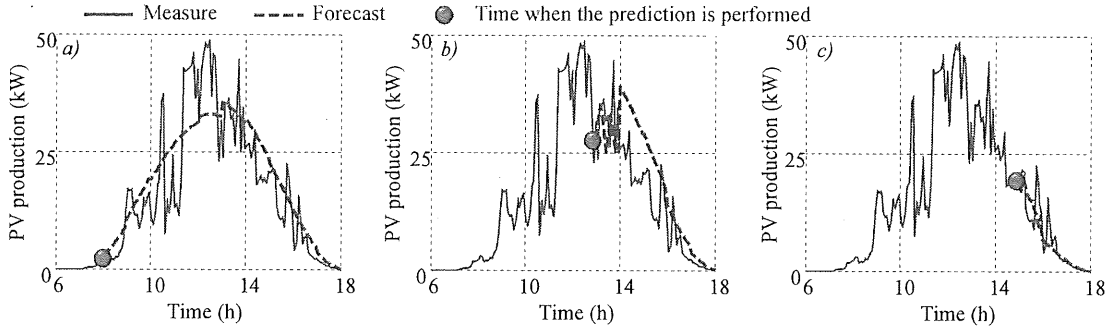

Fig.10: Sample of production forecast – *a)* at 8:00 – *b)* at 13:00 – *c)* at 15:00

500 samples are taken from the testing data and both RMSE and relative error for the prediction are estimated for different time horizon similarly to Eq.5 and Eq.6. Fig.11 displays the prediction error depending on the considered prediction horizon. Note that with the hybrid model the error strongly decreases for the first predicted hour compared to a case in wish the whole profile is predicted using the Weather Underground hourly forecast. Especially the observed error is lower than for a persistent prediction for the first 30 min ahead. With short term prediction uisng kNN the increment of the error with the prediction horizon is also more noticeable. However it ca been observed that the computed values appears to be significant with relative error above 20 % but remain within the range of some performances advised in the literature [Diagne 13].

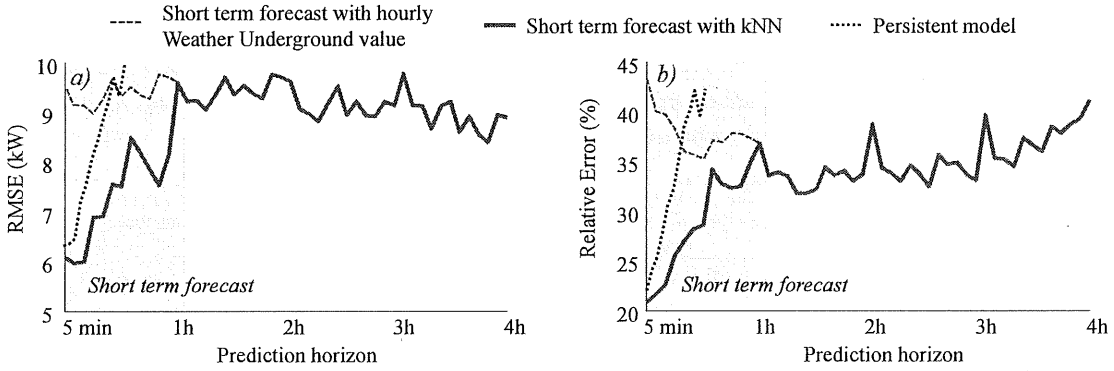

Fig.11: Prediction Error – *a)* RMSE – *b)* Relative Error

3.2.3 Prices

For the purchase energy the UW campus is subject to retail prices from Seattle City Light (http://www.seattle.gov/light/) for "High Demand General Service City" with peak consumption over 10 MW. As detailed in Table 1 two energy rates λ on a day/night basis are set with on On-Peak period from 6:00 to 22:00 and an Off-Peak period from 22:00 to 6:00. Also the peak demand is computed and penalized with a cost λ_{peak} as the maximum average consumption over 15 min within the billing period (typically a month). The Demand Off-Peak is not considered in the study as the peak is expected to occur only during the On-Peak time

Table 1: Energy rates

Energy On-Peak ($/kWh)	$\lambda = 0.0732$
Energy Off-Peak ($/kWh)	$\lambda = 0.0491$
Demand On-Peak ($/kW)	$\lambda_{peak} = 2.08$
Demand Off-Peak ($/kW)	$\lambda_{peak} = 0.22$

Note that as the prices remain constant all over the year no forecast tool is implanted to predict them. However price like transactive signals can randomly occurs without being predicted. Thus in the case study the possibility of introducing instantaneous signals λ_{TS} (typically ±10 $/kWh) is investigated in order to estimates the ability of the system to respond to those unpredicted incentives.

3.3 GAMS Agent

As explained in the first section of the document the management of the system is based on a MPC approach with receding horizon. Every time the optimization process is called the previously mentioned forecasts profile are refreshed before the problem is solved using GAMS. The Python API is used to forward those refresh inputs to GAMS that solves a standard problem written in a ".gms" file. The objective is to minimize the electrical bill on the optimization horizon solving a very basic dispatch problem on the end user side with deterministic load and production (Eq.10). No balance constraints is introduced with the main grid considered as an infinite storage here, while the distinction is made for the charge (resp. discharge) power of the battery P_{bat}^{-} (resp P_{bat}^{+}) in generator convention. In addition to the battery power another variable P_{peak} is introduced in order to take the peak demand penalty into account. Thus the optimization problem finally have $2\times\tau_{pred}+1$ variables (τ_{pred} expressed in number of time steps) with bounds expressed in Eq.11 using the maximum charge (resp. discharge) power $P_{bat\_max}^{-}$ (resp. $P_{bat\_max}^{+}$).

$$\min \text{obj} = \lambda_{peak} \times P_{peak} + \sum_{t=0}^{\tau_{pred}} \left(\lambda(t) + \lambda_{TS}(t)\right) \times \left(P_{load}^{P}(t) - P_{PV}^{P}(t) - P_{bat}^{+}(t) + P_{bat}^{-}(t)\right) \quad \textbf{Eq.10}$$

$$\begin{cases} 0 \le P_{bat}^{+} \le P_{bat\_max}^{+} \\ 0 \le P_{bat}^{-} \le P_{bat\_max}^{-} \\ 0 \le P_{peak} \end{cases} \quad \textbf{Eq.11}$$

The battery system is simply modeled by a linear expression linking the state of charge SOC with the charge/discharge powers and using constant charge/discharge efficiencies (η_{bat}^{+} and η_{bat}^{-}) that represents the loss of both storage and power conversion system (Eq.12). The SOC expressed in % requires considering the time step dT and the maximum energy stored in the battery E_{bat_max} in kWh with upper and lower bounds (SOC_{max} and SOC_{min}) An additional constraints is introduced to ensure that the peak value of the net load P_{peak} corresponds to the actual maximum value computed within the prediction horizon (Eq.13).

$$SOC(t+1) = SOC(t) + \frac{100 \times dT}{E_{bat\_max}} \times \left(\eta_{bat}^{-} \times P_{bat}^{-} - \frac{P_{bat}^{+}}{\eta_{bat}^{+}}\right) \quad \textbf{Eq.12}$$

$$P_{load}^{P}(t) - P_{PV}^{P}(t) - P_{bat}^{+}(t) + P_{bat}^{-}(t) \le P_{peak} \quad \textbf{Eq.13}$$

The optimization problem is solved every $\tau_{refresh}$ with refreshed profiles for the consumption, the production and the prices that cover the prediction horizon. Once the process is over the optimal values P_{bat}^{+*} and P_{bat}^{-*} are used to compute the storage controls P_{bat_ref} (Eq.14). Those controls are sent to the BESS controller as a table. Then the controller reads at each time step the corresponding reference value to send to the battery converter.

$$P_{bat\_ref}(t) = P_{bat}^{+*} - P_{bat}^{-*} \quad \textbf{Eq.14}$$

3.4 Emulated BESS

The proposed management method of the system is based on a MPC approach with a receding horizon implemented in Volttron. The optimal controls generated by the process described in the previous section are sent to the BESS whose behavior won't correspond to the one forecasted due to the

simplification of the model in GAMS (linear formulation with constant efficiencies). Just like the PV arrays, the BESS is not yet installed on the University of Washington campus. Thus, in order to take into account the deviations of the battery characteristics (especially the *SOC*) with the prediction a more detailed model is considered.

3.4.1 Shepherd model for battery cells

The battery cells are represented using the Shepherd model that predicts the component behavior based on the discharge curve at constant C-rate advised by the manufacturers. The model compute the cell voltage V (in Volt) depending on the discharge current I (in A) and the exchanged amper-hours Q (in Ah). Fig.*12a* displays a standard discharge curve for any electrochemical storage cell. After a first exponential decrease, the voltage linearly evolves with the delivered capacity between 80 % and 20 % of the nominal capacity (Q_{nom} in Ah). At the end of the discharge curve (typically under 20 % of *SOC*) the voltage significantly drops to its minimum value [Shepherd 65]. Typically for Li-Ion cells the cell voltage is in the range 2.7 V – 4.0 V with an average value of 3.6 V in the linear area.

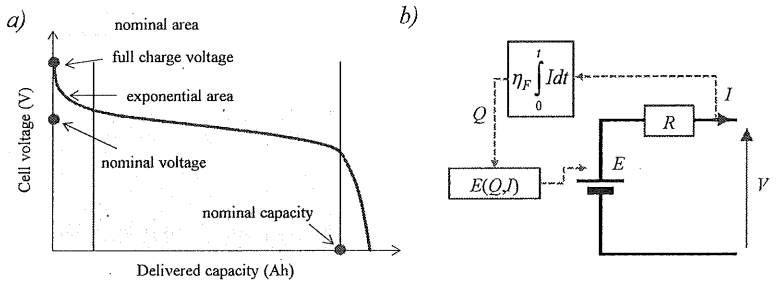

Fig.12: Cell representation – *a)* discharge curve – *b)* Shepherd mode; – *b)* Relative Error

The Shepherd representation of the cell consists in a variable voltage source E in serial with a constant resistance in a generator convention. As shown on Fig.*12b* a faradaic efficiency is added to the base model to represent the electron losses (especially during the charge). For the Li-ion elements that value is close to 1 [Martha 12], a constant η_F = 99.7 % is chosen here for charge (1 / η_F for discharge). [Tremblay 09] improved the Shepherd model originally developed for lead-acid batteries in order to make it compatible for Li-Ion cells in charge ($I < 0$) and discharge ($I > 0$). The function predicting the voltage source value E with the current and capacity is rewritten according to Eq.20. The main assumptions of the model concerns the internal resistance supposed to be constant and the Peukert effect that is not considered. Also the impact of the temperature and the self-discharge are not considered.

$$\begin{cases} I > 0 \Rightarrow V = E_0 - R.I - K_{dr}.Q.\dfrac{Q_{nom}}{Q_{nom} - Q} - K_{dv}.I.\dfrac{Q_{nom}}{Q_{nom} - Q} + A.e^{-B.Q} \\ I < 0 \Rightarrow V = E_0 - R.I - K_{cr}.Q.\dfrac{Q_{nom}}{Q_{nom} - Q} - K_{cv}.I.\dfrac{Q_{nom}}{Q - 0.1.Q_{nom}} + A.e^{-B.Q} \end{cases} \quad \textbf{Eq.15}$$

With:

- E_0 : battery constant voltage (V)
- R :internal resistance (Ω)
- A : exponential zone amplitude (V)
- B : exponential zone time constant inverse (Ah^{-1})
- K_{dr}, K_{cr} :polarization resistance (Ω)
- K_{dv}, K_{cv} :polarization constant (V/Ah)

As already explained and shown on Fig.*12b* the capacity delivered by the battery is computed by considering the faradaic efficiency (Eq.16). Then Eq.17 is used to estimate the *SOC* of the cell that depends on the remaining capacity that can be delivered.

$$Q(t) = \eta_F \times \int_0^t I.dt \text{ with } \begin{cases} I < 0 \Rightarrow \eta_F = 99.7\% \\ I > 0 \Rightarrow \eta_F = 1/99.7\% \end{cases} \quad \textbf{Eq.16}$$

$$SOC(t) = 100 \times \frac{Q_{nom} - Q(t)}{Q_{nom}} \quad \textbf{Eq.17}$$

3.4.2 Parameters fitting

Normally the parameters of the model can be extracted from the discharge curves. Here the choice is made to fit the parameters using the least square minimization tool embedded in Matlab in order to find the values for E_0, A, B, R. As described in [Tremblay 09] the polarization constant in charge and discharge are supposed to have the same values denoted as K here. Also note the BESS that is going to be installed on site will be composed of LGchem modules. Unfortunately the discharge curves are not available for the corresponding cells. Thus other products with extensive datasheet are considered with the Li-ion cells VL45E used in the solutions for stationary storage provided by SAFT (See Appendix D). The corresponding nominal capacity is equal to 45 Ah with a cell voltage between 2.7 V and 4.0 V and the discharge curves are given at 22.5 A (C/2), 45 A (1C) and 100 A (>2C).

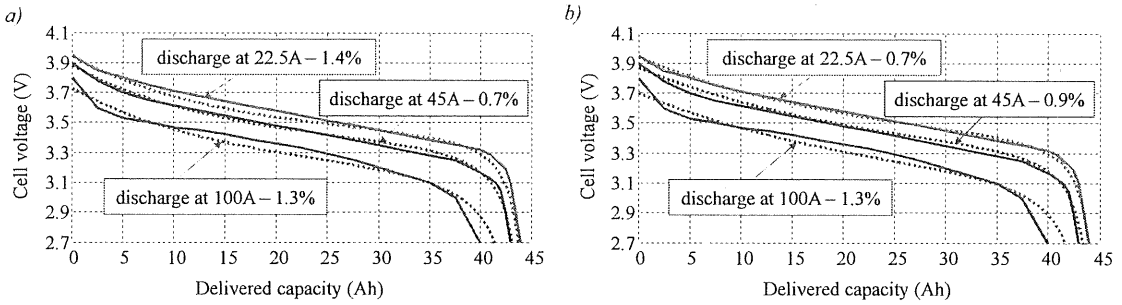

Fig.13: Fitting relative errors – *a)* fitting discharge at 1C – *b)* fitting discharge at C/2, 1C and 100A

Two fitting strategies are considered and the obtained solutions are compared in term of relative error computed similarly to Eq.6. At first only the discharge at nominal c-rate is considered. The obtained error is very low for the discharge at 1C but it increases a little when predicting the discharge at C/2 and 100 A (Fig.13*a*). Another approach consists in fitting the three curves at once. In this case the error for the discharge at 1C is slightly higher but it decrease significantly for C/2 (Fig.13*b*). Table 2 displays the values of the parameters for the two fitting strategies. In the following parts the results for the fitting of the three curves will be considered.

Table 2: Energy rates

Parameter	Fitting 1C	Fitting C/2, 1C and 100 A
E_0 (V)	3.50	3.43
R (Ω)	$2.5.10^{-3}$	$2.8.10^{-3}$
A (V)	0.50	0.57
B (Ah^{-1})	$7.51.10^{-2}$	$4.96.10^{-2}$
K (Ω and V/Ah)	$3.27.10^{-4}$	$2.74.10^{-4}$

Once the parameters are computed the model for a single cell can be used to simulate the behavior of the product with different current profiles. Appendix E displays the results obtained for charge/discharge a 1C and estimates the round trip efficiency of the considered cell. Especially the charge mode is investigated with a saturated voltage and decreasing current introducing a time of fully charge longer than the one computed with a standard ideal model.

3.4.3 From cells to battery

For the design of energy storage system, manufacturers define elementary module usually composed of cells in series. Different modules are then arrange in parallel and series to construct the battery rack depending on the desired overall voltage and current rate (Fig.14). The proposed BESS that is going to be installed on the UW campus is given with a rated energy of 325 kWh and a power conversion system with a maximum power of 100 kW. Note that in those conditions the battery would be operated at lower c-rates which could allow reducing the losses while increasing the system lifespan.

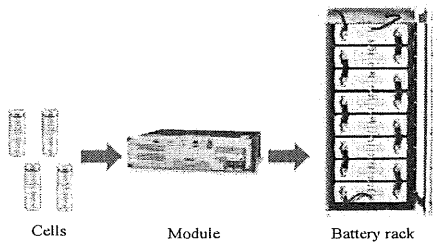

Fig.14: Battery modules

To emulate the overall BESS the previously modeled cells are associated in series N_{serie} and parallel N_{parat} assuming that all the components are balanced in terms of voltage and state of charge. The SAFT cells is given with a specific energy of 162 Wh at the nominal voltage (3.6 V). With no additional information on the BESS design, the choice is arbitrary made to use N_{serie} = 200 and N_{para} = 10 for a battery nominal voltage of 720 V and an estimated rated power of 324 kW. Thus starting from the references controls return by the optimization P_{bat_ref} the reference current for a single cell is computed using the voltage for the previous time step. Then the developed model predicts the new value for a single cell voltage and refreshes its *SOC* which is assumed to represent the battery *SOC*. The other battery parameters I_{bat} and V_{bat} are then computed following the model architecture on Fig.15. Note that a constant efficiency is added to represent the losses within the converter (η_{cvs} = 95 %).

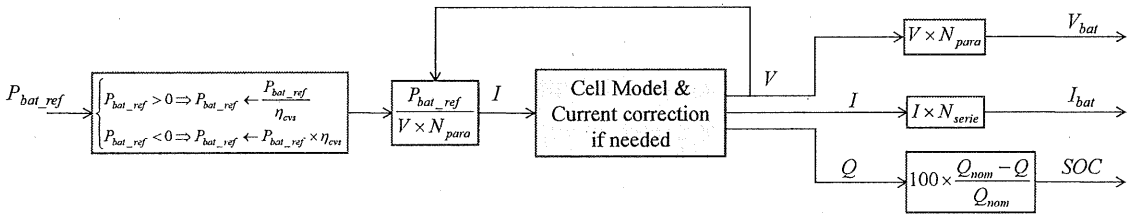

Fig.15: Model architecture for the battery

The proposed architecture requires to compute the cell/battery voltage for the initial time step. The open voltage versus *SOC* curve provided by the manufacturer is used to compute the initial voltage V_{init} with the initial state of charge SOC_{init} of the cells using Eq.18.

$$V_{init} = \frac{SOC_{init}}{100} \times 0.7 + 3.3 \qquad \textbf{Eq.18}$$

4 SIMULATIONS

4.1 Case study

The proposed management method with the implemented models described in the previous section is simulated for a day of September 2016 with the load and production profiles displayed on Fig.16. For a baseline case without PV nor battery, the peak consumption is 898 kW for a total purchase energy of 20 MWh. The optimization is performed every $T_{refresh}$ = 30 min and the prediction horizon stops at the end of the day with forecast profiles (production, load and prices) ending at midnight. Note that the developed forecast tool for temperature and solar radiation require the past time steps measurements to predict the short term values. Thus when simulating a single day the management process cannot be start at 0:00. Here the choice is made to "switch on' the MPC controller at 2:00.

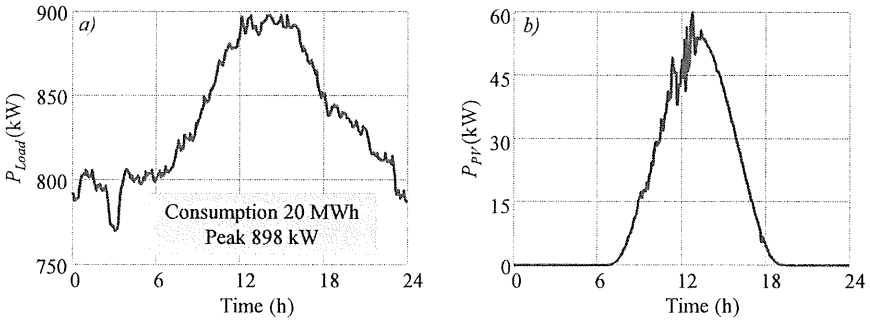

Fig.16: Test profiles – *a)* Load – *b)* PV production

In the MPC controller the simple linear model of the BESS is set with P_{bat_max}=−P_{bat_min}=100 kW with a maximum energy E_{bat_max} equals to 325 kWh. Also both charge and discharge efficiency (η_{bat}^{+} and η_{bat}^{-}) are set to 90 %, SOC_{max} = 100 % and SOC_{min} = 20 %. Also the BESS is assigned with an initial *SOC* of 50% and an additional constraint is introduced to ensure that its final value is over (SOC(24 h) ≥ SOC(0 h)). That constraint allows avoiding a fully discharged battery at the end of the day and returning to the initial value favors the conservativeness of the operation.

4.2 Results

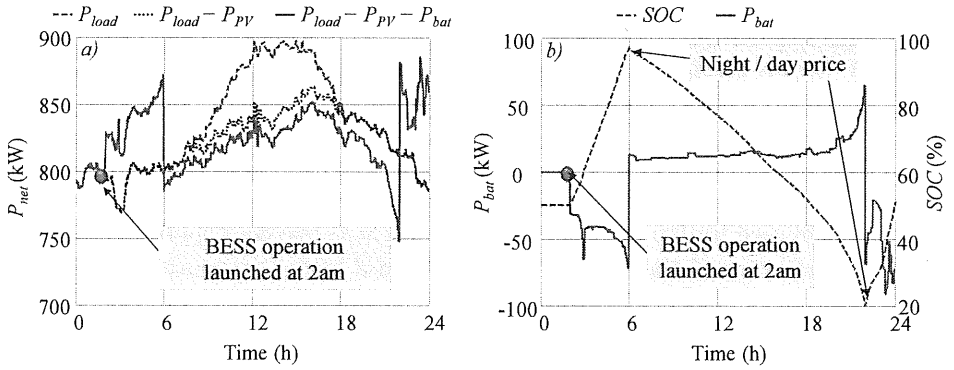

Fig.17: Results considering only the arbitrage – *a)* net load – *b)* BESS profiles

A first simulation is performed while removing the peak consumption penalty in the cost function embedded in the MPC controller (Eq.10). In that case the consumption tends to increase during the off-peak period (until 6:00) with a full charge of the battery. Then when the prices for the purchased energy are higher during the day, the BESS slowly discharges to its lower limit (i.e. 20 %) before the prices get lower at 22:00 (Fig.17). At the end of the day the storage is then charge until reaching the specified value *SOC*(24 h). On the displayed profiles the start time of the battery management can also be observed with no controls sent to the storage until 2:00.

Table 3: Simulation results

Simulation	Purchase Energy ($)	Peak Penalty ($)	Total ($)
Baseline – load	1313	1868 - (898 kW)	3131
Baseline – load and PV	1290	1795 - (863 kW)	3085
BESS - arbitrage	1286	2841 - (885 kW)	3127
BESS – arbitrage + peak	1288	1781 – (857 kW)	3069
BESS – arbitrage + peak + TS	1289	1917 – (921 kW)	3206

As summarized in Table 3 the cost for the purchase energy is reduced compared to a baseline where only the load is considered. However 85 % of that decrement is cause by the PV production. With small difference between day and night rates, the BESS operation only allows saving 4 $ more. The peak power occurs during the off-peak period (the cost for on-peak is applied) and is higher than in a case where only the load and the production are considered. Note that the penalty attached to the peak power is computed here for the simulated day. Normally it is only applied for the highest observed values within the billing period, typically a month.

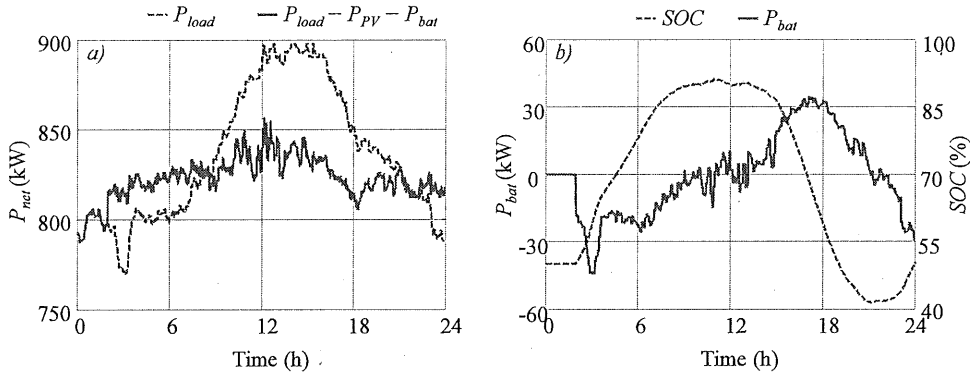

Fig.18: Results considering arbitrage and peak penalty– *a)* net load – *b)* BESS profiles

Another simulation is performed while considering the peak penalty in the objective function of the MPC controller. In that case the observed peak power is significantly decrease to 856 kW with a cost for the purchased energy slightly increased and a lower total bill (Table 3). Nate that compared to the previous case, the BESS is not used in all the available range with a *SOC* that does not reach the upper and lower bound (Fig.18*b*). Indeed increasing the *SOC* would led to a higher net power and a more significant corresponding peak consumption. Then the penalty paid would be more important than the saving obtained with a more efficient arbitrage between off-peak and on-peak periods.

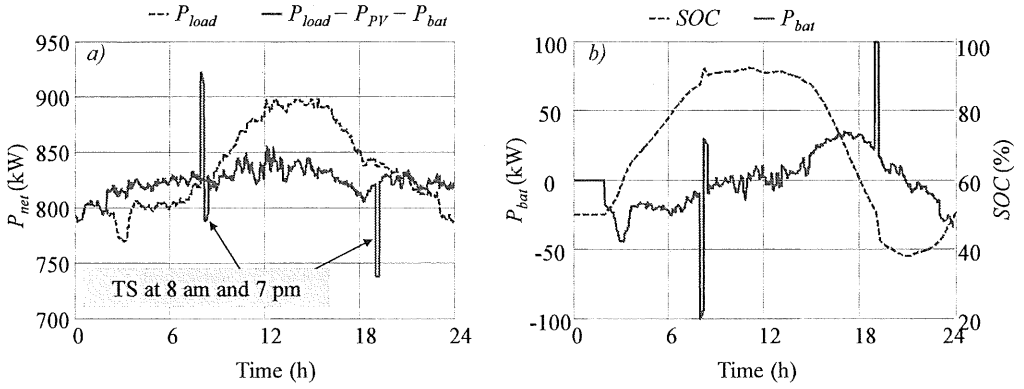

Fig.19: Results considering arbitrage and peak penalty with TS – *a)* net load – *b)* BESS profiles

A last simulation considers the occurrence of unpredicted transactive signals, $\lambda_{TS} = -10$ \$/kWh at 8:00 am and $\lambda_{TS} = 10$ \$/kWh at 7:00 pm. Those values are added to the rates profile for three consecutive time steps (i.e. 15 min). The corresponding profiles are displayed on Fig.23 with a BESS that proves able to respond to the transactive signals. The battery absorbs and provides power that reaches the specified bounds P_{bat_max} and P_{bat_min} while speeding up the charge/discharge. Note that the peak power for the net consumption is much higher than in the previous simulations (911 kW) with a total cost significantly increased (Table 3). Thus the retribution for an increased consumption (i.e. negative TS here) should compensate the penalty for the corresponding peak. Otherwise the battery would operate at a charge rate that would limit the net consumption to the predicted maximum possible value.

4.3 Discussion

4.3.1 Forecast refreshment

An additional set of simulations is performed considering the peak penalty without TS and varying the refreshment period for the MPC controller. As shown in Table 4 changing the value of the intra-hourly refreshment does not have a significant impact on the obtained results. Also the corresponding performances (in terms of cost) are significantly better than the results observed with no refreshment of the optimal control (i.e. $T_{refresh} = 24$ h with the optimization performed only one time). However refreshing the optimization does not allow in any case reaching the minimum peak power computed at 824 kW with the given measured profiles. Indeed the refreshment process does not allow to perfectly manage the load and production uncertainties.

Table 4: Simulation results with different values of $T_{refresh}$

$T_{refresh}$	5 min	15 min	30 min	1 h	24 h
Purchase Energy (\$)	1288	1288	1288	1288	1290
Peak Penalty (\$)	1785 – 858 kW	1780 – 856 kW	1781 – 857 kW	1781 – 857 kW	1798 – 864 kW
Total (\$)	3073	3068	3069	3069	3088

In order to improve the performances of the proposed procedure a real time controller can be added to the rolling windows optimization. The simplest way to cancel the uncertainties compared to the predicted refreshed profiles would consist at correcting the BESS real time control as described in Eq.19.

$$P_{bat\_ref} \leftarrow P_{bat\_ref} + P_{load}(t) - P_{PV}(t) - P^{P}_{load}(t) + P^{P}_{PV}(t) \qquad \textbf{Eq.19}$$

A last new simulation is run with $T_{refresh}$ and the simple real time correction described above. Once again no TS in considered. The observed final cost is the lowest one obtained for the tested day with 3046 $ total and a peak power reduced from 857 kW to 845 kW. Also the corresponding net power profile appears to be smoother compared to the previous studied cases with constant values over refreshment period of 30 min here (Fig.20*a*). As the uncertainties are non-biased the deviations of the *SOC* compared to a case with no real time correction are not significant (Fig.20*b*).

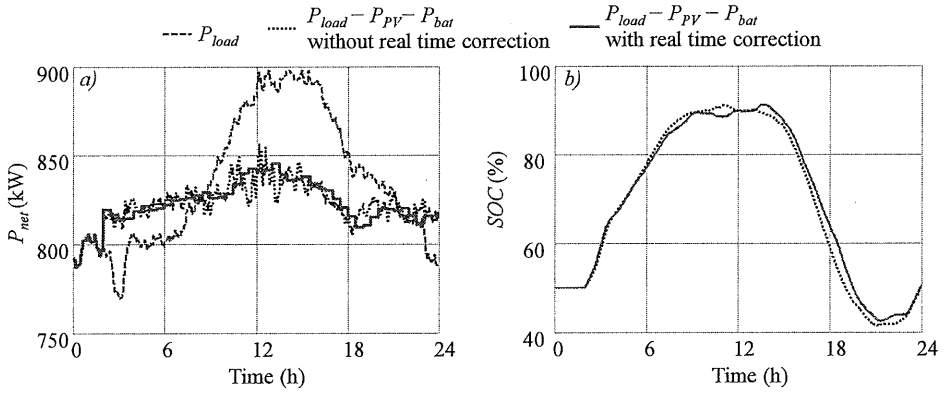

Fig.20: Results with and without real time correction – *a)* net load – *b) SOC* profiles

4.3.2 BESS limitations

As already mentioned the BESS is represented with a simple linear model in the MPC controller. Thus is some cases the actual equipment would not be able to meet the sent controls in some cases. Fig.21 displays the profiles for the first case simulated where only the arbitrage was considered. Especially at the end of the storage charge before 6:00 am the purchased power cannot meet the references due to the battery dynamics at higher *SOC* values (see Appendix E). In real time with actual modules, such a phenomenon could occurs when the battery management system would limit the use of the storage with maximum real time charge/discharge current, cell voltage imbalances or overheating.

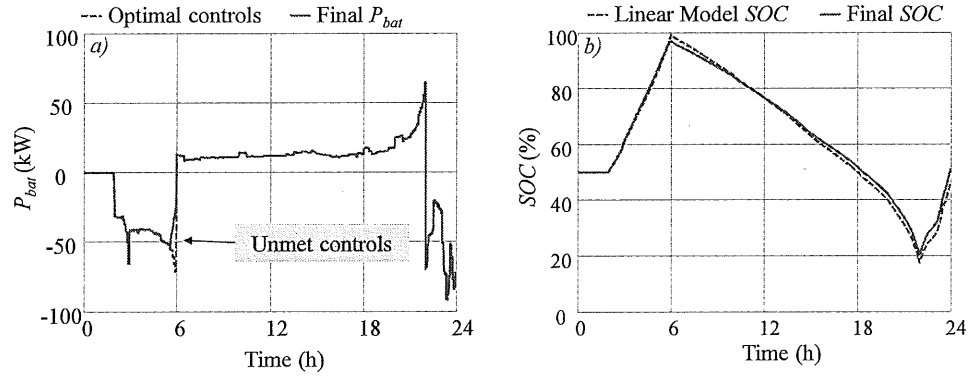

Fig.21: Results with and without real time correction – *a)* net load – *b) SOC* profiles

CONCLUSIONS

This report presents the use of a multi-agent platform to implement a management strategy for a BESS associated with PV production. Especially attention has been paid to the generation of consumption and production forecast that are used by the MPC controller when the optimization is performed on a rolling windows. For the tested day the proposed approaches proved itself performant, especially with a decreased net load that led to a significant reduction of the electrical bill. As discussed the BESS operation can be enhance especially by introducing a real time controller that would allow smarter operation (follow a target power, smooth the net load). A basic example has been given in the document but other approaches should be investigated. Among the possible further work the main task is obviously to deploy the proposed strategy on the real system using the Volttron platform when the equipment will arrive.

APPENDIX A: PV MODULES DATASHEET AND PV SYSTEM

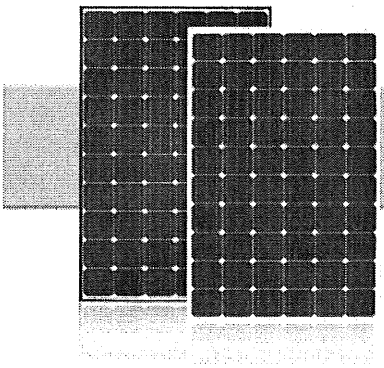

itek ENERGY HE SOLAR MODULES

PERFORMANCE - QUALITY - AFFORDABLE

- BUILT IN WASHINGTON USING CUTTING EDGE HIGH EFFICIENCY MONOCRYSTALLINE CELLS
- 25 - YEAR POWER OUTPUT WARRANTY
- 10 - YEAR WORKMANSHIP WARRANTY
- EXCEPTIONAL POWER DENSITY (W/m^2)

GENERAL DATA

Cell type	• 60 high-efficiency monocrystalline p-type cells • 6x10 cell matrix
Solar Glass	• Ultra-clear anti-reflective treatment • Tempered, with low iron content • Anti-glare prismatic subsurface texture
Backsheet	• Multi-layered • Engineered adhesion for maximum weather protection
Frame	• High-strength corrosion-resistant anodized aluminum • Compatible with standard racking, accommodating both top-down clamps and bottom-flange mounting • Micro-inverter and DC optimizer attachment points
Cable	• 47" 90C 12 AWG PV wire • 1000 VDC MC4 connector wire
Junction Box	• 3 bypass diodes
Grounding	• Certified for Wiley Electronics WEEB™ grounding clips • Eight standard grounding locations per module for reduced ground wire length

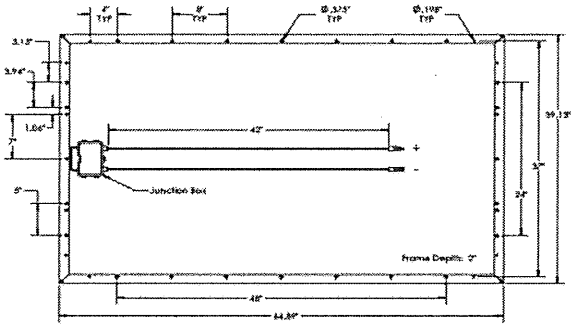

MECHANICAL DATA

Dimensions	39.17" X 64.8" X 2"
Weight	43 lbs

MAXIMUM RATINGS

Operational Temperature	-40...+ 90°C
Maximum System Voltage	1000 VDC
Design Load (UL 1703)	up to 113 lbs/ft²
Maximum Load (UL 1703)	551 kg/m² (5400 Pa)
Maximum Wind Load	113 lbs/ft²
Max Series Fuse Rating	15A
Max Reverse Current	15A

NOTE: SPECIFICATION IS SUBJECT TO CHANGE WITHOUT NOTICE

TEMPERATURE RATINGS

Nominal Operating Cell Temperature (NOCT)	46.20 °C
Temperature Coefficient of P_{MPP}	- 0.47 %/°C
Temperature Coefficient of V_{OC}	- 0.32 %/°C
Temperature Coefficient of I_{SC}	+ 0.04 %/°C
Temperature Coefficient of V_{MPP}	- 0.45 %/°C

QUALIFICATIONS

UL Listing	UL 1703
Fire Rating	Type 2

Certified Made in Washington

Intertek

itek ENERGY

Building Solar | Powering The Future

itekenergy.com | WA. 360.647.9531 MN. 612.318.6369

ELECTRICAL DATA*

	270 HE	275 HE	280 HE	285 HE	290 HE	295 HE	300 HE	305 HE	310 HE
Maximum Power - P_{max} (Wp)	270	275	280	285	290	295	300	305	310
Maximum Power Voltage - V_{MPP} (V)	32.0	32.1	32.3	32.4	32.6	32.8	32.9	33.1	33.2
Maximum Power Current - I_{MPP} (A)	8.4	8.5	8.6	8.7	8.8	8.9	9.0	9.1	9.2
Open Circuit Voltage - V_{OC} (V)	38.9	39.0	39.2	39.3	39.5	39.7	39.8	40.0	40.1
Short Circuit Current - I_{SC} (A)	9.1	9.2	9.3	9.4	9.5	9.6	9.7	9.8	9.9
Module Efficiency	16.49%	16.80%	17.10%	17.41%	17.71%	18.02%	18.32%	18.63%	18.94%

*Electrical characteristics may vary within ±3% of the indicated values at Standard Test Conditions(STC): irradiance of 1,000W/m2, AM 1.5 spectrum, cell temperature at 25°C (77°F)

V09.01.16

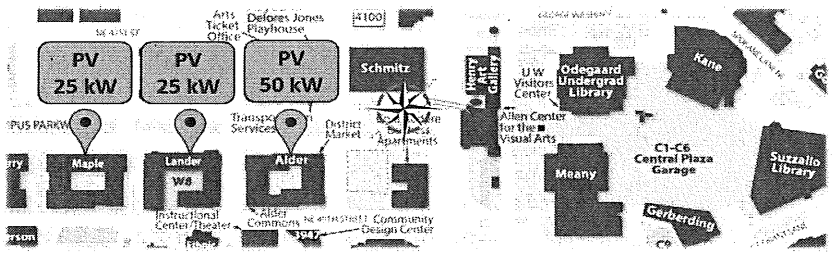

APPENDIX B: SOLAR ANGLES

This appendix presents the different steps to the compute the solar angles (elevation α_e and azimuth α_a) that are used to correct the solar radiation on a collector with given tilt θ_t and orientation θ_o. The corresponding equations (Eq.20 to Eq.24) are taken from [Masters 13].with the following parameters:

- δ : solar declination
- L :latitude
- n : day number
- H : hour angle
- α_e :elevation angle
- α_a : azimuth angle (< 0 for West from South, > 0 for East from South)

$$\delta = 23.45 \times \sin\left(\frac{360}{365} \times (n - 81)\right) \quad \textbf{Eq.20}$$

$$H = 15^O \text{ per hour before solar noon (mind time shift summer/winter time)} \quad \textbf{Eq.21}$$

$$\sin\alpha_e = \cos L \times \cos\delta \times \cos H + \sin L \times \sin\delta \quad \textbf{Eq.22}$$

$$\sin\alpha_a = \frac{\cos\delta \times \sin H}{\cos\beta} \quad \textbf{Eq.23}$$

$$\text{If } \cos H < \frac{\tan\delta}{\tan L} \text{ then } \alpha_a \leftarrow 180^O - \alpha_a \quad \textbf{Eq.24}$$

With the previous equations it becomes possible to plot the sun path diagram depending on the geographical position. Fig.22*a* displays the obtained curve in Seattle for seven different day from June to December with a maximum elevation angle moving from 20^O to 65^O. On Fig.22*b* the corrected factor for the irradiance on a collector is plot for different tilt and orientation angles (positive orientation, East from South). For the considered day in October the optimal tilt corresponds to 57^O with variations from 0.5 to 1. The observed effect of non-optimal orientations is around 10 % for the tested values.

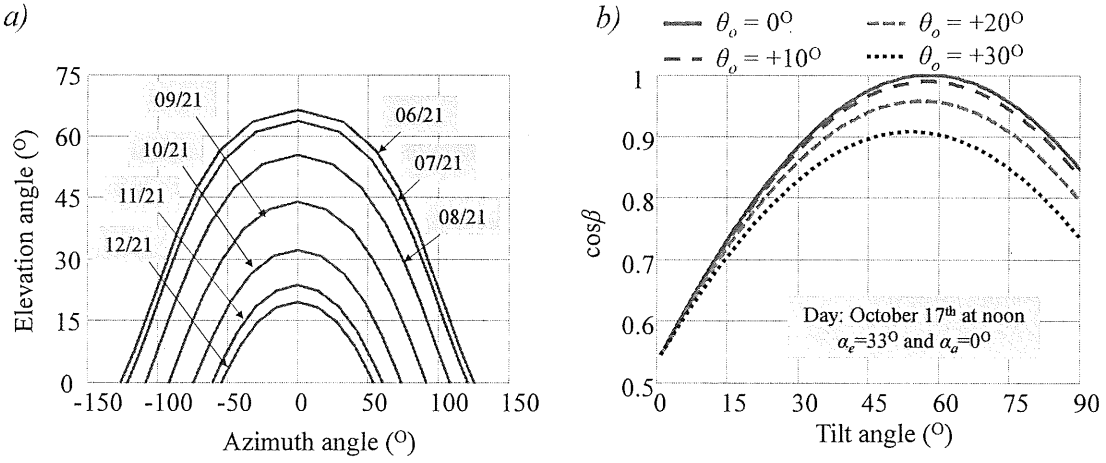

Fig.22: Solar curves – *a)* solar position for different day – *b)* angle of incidence on a collector with different tilt and orientation angles

APPENDIX C: kNN PARAMETERS

This appendix investigates different parameters for the short term forecast tool using the k Nearest Neighbor method for PV production. Thus for both the temperature and clarity index predictors, different test are performed with several values regarding the number of considered nearest neighbor (k) as well as the length of the measurement used to compute the forecast (τ_{lag}). The RMSE and relative error are compute considering 500 samples within the test period (September 20616) with different prediction horizon τ_{pred}. Fig.23*a* and Fig.23*b* display the errors plot by varying k and with τ_{lag} fixed at 30 min for the solar radiation predictor. As expected the observed error tends to increase with the prediction horizon with values around 20 % for 30 min ahead forecast. Increasing the number of considered nearest neighbors improve the performance with a limit values reached for $k = 10$. Keeping that value and varying τ_{lag} from 15 min to 2 h have less significant impact on the computed errors that slightly increase when longer measurement profile are considered to perform the prediction (Fig.23*c* and Fig.23*d*).

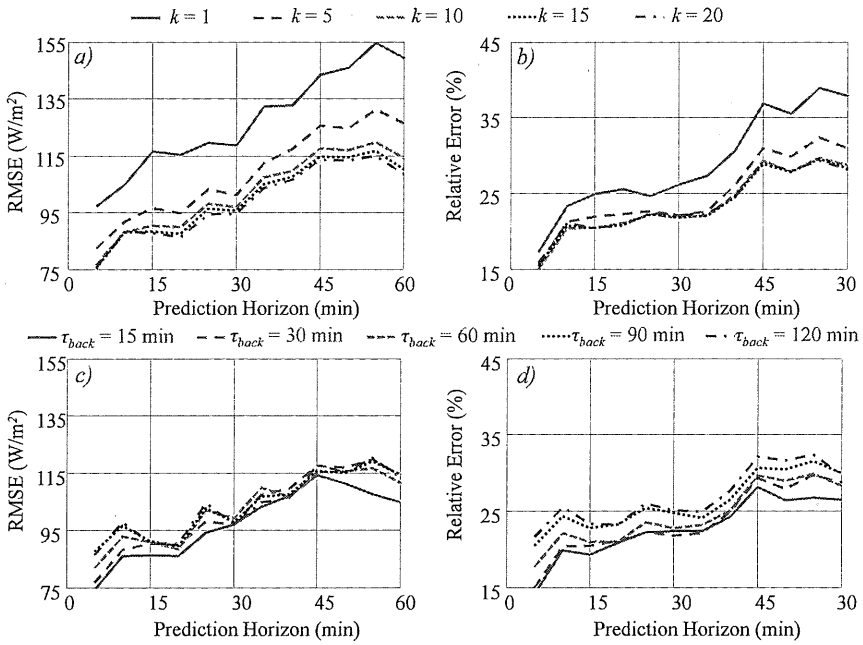

Fig.23: Solar radiation predictor– *a)* RMSE with different k – *b)* relative error with different k – *c)* RMSE with different τ_{lag} – *d)* relative error with different τ_{lag}

For the temperature the observed errors are much smaller. The impact of k and with τ_{lag} fixed at 30 min is more random than for the clarity index (Fig.24*a* and Fig.24*b*). Here again increasing τ_{lag} tends to slightly increase the error (Fig.24*c* and Fig.24*d*). In the presented work k is set to 10 and τ_{lag} at 15 min (i.e. 3 time steps here). Note that finding optimal value for predictor model could also be formulated as an optimization problem.

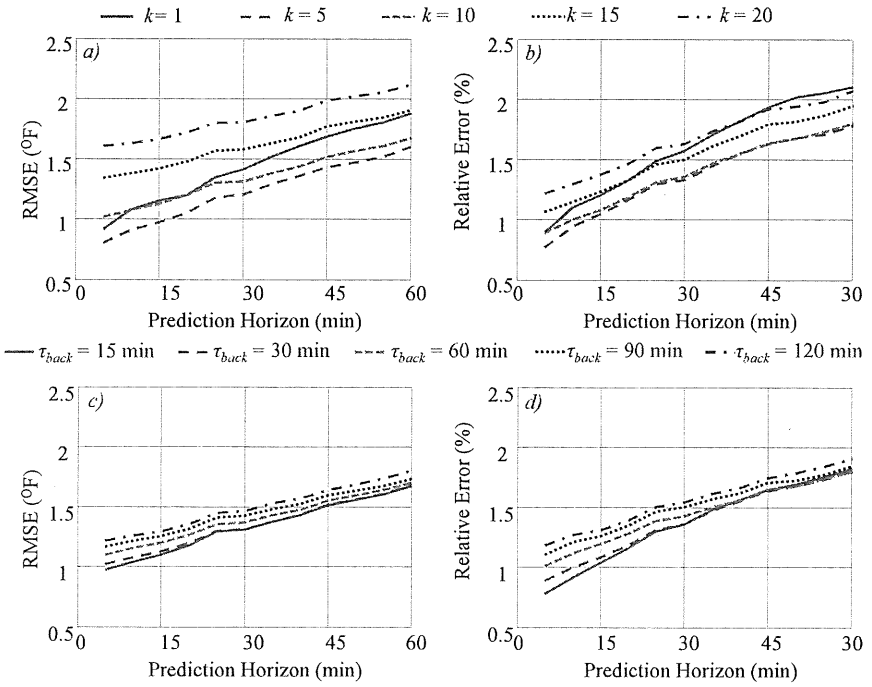

Fig.24: Temperature predictor– *a)* RMSE with different k – *b)* relative error with different k – *c)* RMSE with different τ_{lag} – *d)* relative error with different τ_{lag}

APPENDIX D: LI-ION CELL DATASHEET

High energy lithium-ion cell
VL 45 E cell

Saft VL E cell is highly suited to any charge/discharge cycling application that demands a battery with drastically reduced weight and volume. This cell is proposed in Saft modules or customized battery system constructions.

Saft's Battery system :
Individual lithium-ion cells need to be mechanically and electrically integrated into battery systems to operate properly. The battery system include electronic devices for performance, thermal and safety management specific to each application.

Features
- Very high specific energy
- Maintenance free
- Excellent cycle and calendar life

Applications
- Electric and hybrid vehicles
- Telecommunication networks
- Stationary
- Space and Defence
- Any application requiring high energy storage capability

Technology
- Graphite-based anode
- Nickel oxide-based cathode
- Electrolyte: blend of carbonate solvents + LiPF6

	VL 45 E
Electrical characteristics	
Nominal voltage (V)	3.6
Average capacity C/3 after charge to 4.0 V/cell (Ah)	45
Minimum capacity C/3 after charge to 4.0 V/cell (Ah)	42
Specific energy after charge to 4.0 V/cell (Wh/kg)	149
Energy density after charge to 4.0 V/cell (Wh/dm³)	313
Specific power (30s peak/50% DOD) (W/kg)	664
Power density (30s peak/50% DOD) (W/dm³)	1392
Mechanical characteristics	
Diameter (mm)	54.3
Height (mm)	222
Typical weight (kg)	1.07
Volume (dm³)	0.51
Voltage limits	
Charge (V)	4.0 (4.1 for peak)
Discharge (V)	2.7 (2.3 for peak)
Current limits	
Max continuous current (A)	100
Max peak current during 30 s (A)	250

saft

High energy Li-ion
VL 45 E cell

Cell capacity and voltage according to current at -20°C

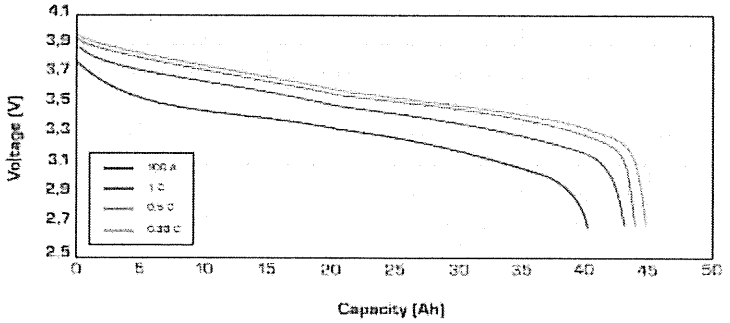

Available capacity after storage charge at 4.0 V

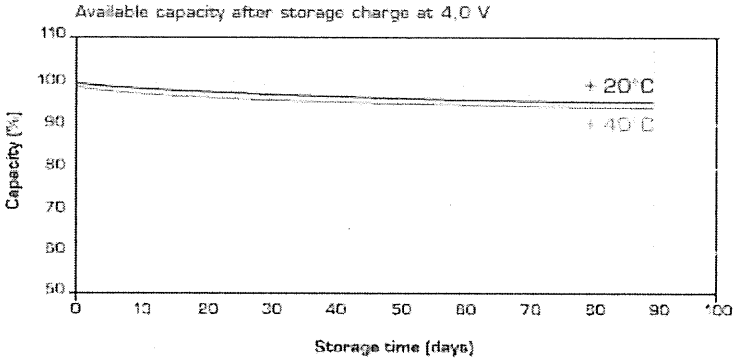

Cycling life in DST profil at 80% of DOD at -20°C. Energy in discharge at C/3 rate and power 30s at 250 A at 50% of S.O.C.

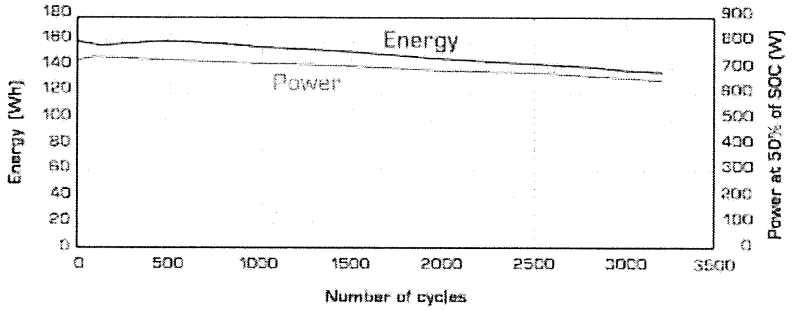

Saft
Communication Department
12, rue Sadi Carnot
93170 Bagnolet - France
Phone: +33 (0)1 49 93 19 18
Fax: +33 (0)1 49 93 19 68

www.saftbatteries.com

DOC N° 54041-2-0305
Edition: March 2005

APPENDIX E: LI-ION CELL MODEL

This Appendix presents the results obtained when using the Li-on cell model developed in the document for the 45 Ah SAFT cell. At first a full cycle 0 %→ 100 % → 0 % at 1C (i.e. 45 A) is simulated considering Eq.20 to Eq.17 while bounding the cell voltage between 2.7 V and 4 V. Fig.25 displays the corresponding profiles for the voltage, the power and *SOC*. The power allows computing both charged and discharged energy that are different due to the distinct voltage trajectories. The ratio between those values gives the round trip efficiency which is 91 % for a cycle at 1C. The performance increase with a low c-rate (95 % for a C/2 cycle) and decreases for higher currents (83 % for a 100 A cycle - >2C).

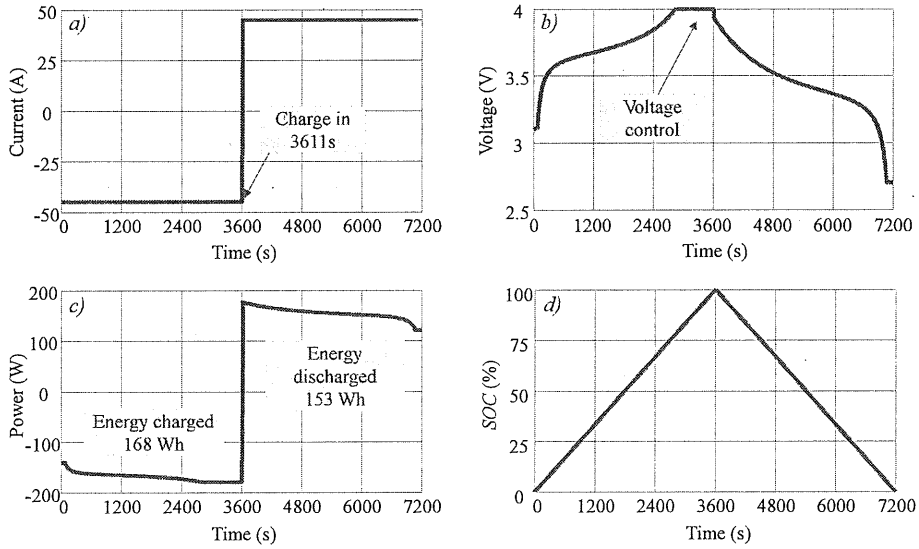

Fig.25: Cell cycling profiles – *a)* current – *b)* voltage – *c)* power – *d) SOC*

In the previous simulation the cell is charge in a little more than one hour - 3611 considering the faradaic efficiency. The corresponding *SOC* moves for 0 % to 100 % with a unrealistic constant current even when the voltage is controlled (at 4 V for instance) for safety reason (venting). In practice the current decreases (in magnitude) when the maximum cells voltage is reach and controlled to its maximum value. Thus the charge is slowed down and reaching an actual *SOC* of 100 % takes much more than an hour even for a c-rate equals to one. Then if a reference current I_{ref} is desired, the actual value I as to be corrected as in Eq.25.

$$I_{ref} < 0 \Rightarrow V = E_0 - R.I_{ref} - K.Q.\frac{Q_{nom}}{Q_{nom} - Q} - K.I_{ref}.\frac{Q_{nom}}{Q - 0.1.Q_{nom}} + A.e^{-B.Q}$$

$$V > 4 \Rightarrow V \leftarrow 4 \text{ and } I = \max\left(I_{ref}, \frac{E_0 - V - K.Q.\frac{Q_{nom}}{Q_{nom} - Q} + A.e^{-B.Q}}{R + K.\frac{Q_{nom}}{Q - 0.1.Q_{nom}}} \right) \qquad \textbf{Eq.25}$$

The comment addressed above can be transposed to the discharge mode. Indeed if the reference current I_{ref} would led to a voltage under the lower bound its magnitude is reduced in order not to damage the cell. Thus the power deliverd by the battery is lowered and the discharge is slowed down compared to the previous test with the corrected equation Eq.26.

$$I_{ref} > 0 \Rightarrow V = E_0 - R.I_{ref} - K.Q.\frac{Q_{nom}}{Q_{nom} - Q} - K.I_{ref}.\frac{Q_{nom}}{Q_{nom} - Q} + A.e^{-B.Q}$$

$$V < 2.7 \Rightarrow V \leftarrow 2.7 \text{ and } I = \min\left(I_{ref}, \frac{E_0 - V - K.Q.\frac{Q_{nom}}{Q_{nom} - Q} + A.e^{-B.Q}}{R + K.\frac{Q_{nom}}{Q_{nom} - Q}} \right) \quad \textbf{Eq.26}$$

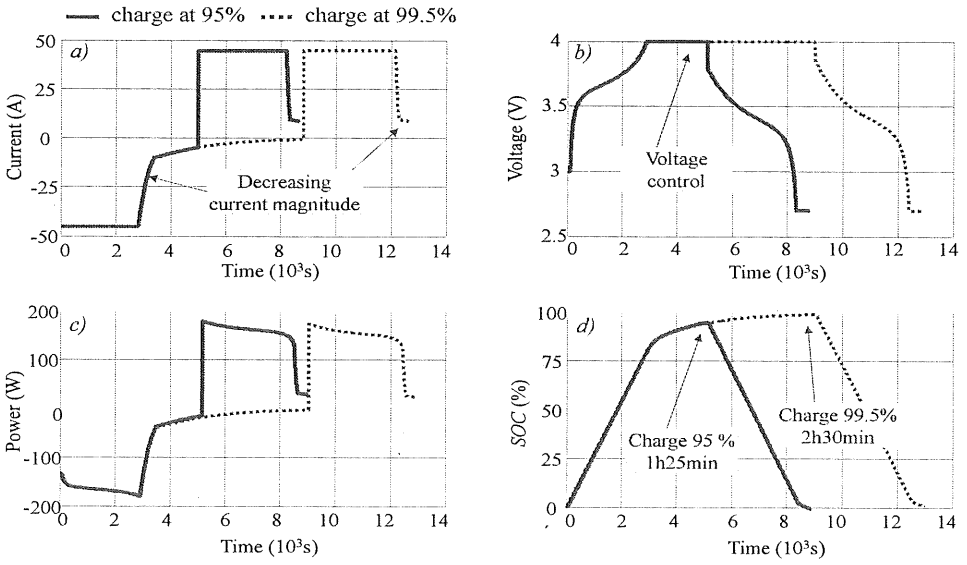

Fig.26: Cell cycling profiles with charge control – *a)* current – *b)* voltage – *c)* power – *d) SOC*

Fig.26 shows the results obtained for a cycle at 1C (i.e. 45 A) with the charge controller with two charges at 95 % and at 99.5 %. As previously the charge current is constant at the beginning of the cycle. Then when the maximum voltage is reached it is maintained to its upper bound (Fig.26*b*) while the current decreases following a negative exponential trajectory (Fig.26*a*). The charge is slowed down, at 1C it takes 1h30min to reach 95 % and more than 2h30min for 99.5 % compared to one hour in a standard ideal model (Fig.26*d*). Also at the end of the profile the simulation the discharge current magnitude is decreased to avoid critical under-voltages (Fig.26*a*) with a discharge slowed down (Fig.26*d*). Note that the computed values for round trip efficiency are consistent with the one previously estimated at 91 % for a cycle at 1C.

REFERENCES

Kantamneni 15	W.Kantamneni, L. E.Browna, G. Parker, W. W.Weaver, "Survey of multi-agent systens for microgrid control", Engineering Application of Artificial Inteligence, Vol 45, pp 192-203, 2015.
Zhang 16	X. Zhang, A. J. Flueck, C. P. Nguyen, "Agent-based distributed volt/var control with distributed power flow solver in smart grid", IEEE Transactions on Smart Grid, Vol 7, pp 600-607, 2016.
Labeodan 15	T. Labeodan, K. Aduda, G. Boxem, W. Zeiler, "On the application of multi-agent systems in buildings for improved building operations, performance and smart grid integration – A survey", Renewable and Sustainable Energy Reviews, Vol 50, pp 1405-1414, 2015.
Haack 13	J.N. Haack, B.A. Akyol, S. Katipamula, R.G. Lutes, "VOLTTRON Lite: Integration platform for the transactional network", Report Pacific Northwest National Laboratory, 2013.
Khamphanchai 14	W. Khamphanchai, A. Saha, K. Rathinavel, J.N. Haack, B.A. Akyol, "Conceptual architecture of building energy management open source software (BEMOSS)", Innovative Smart Grid Technologies Conference Europe (ISGT-Europe), 2014.
Hao 16	H Hao, C.D. Corbin, K. Kalsi, R.G. Pratt, "Transactive Control of Commercial Buildings for Demand Response", IEEE Transactions on Power Systems, 2016.
Darras 10	C. Darras, S. Sailler, C. Thibault, M. Muselli, P. Poggi, J.C Hoguet, S. Melsco, E. Pinton, S. Grehant, F. Gailly, C. Turpin, S. Astier and G. Fontès, —Sizing of photovoltaic system coupled with hydrogen/oxygen storage based on the ORIENTE model, International Journal of Hydrogen Energy, Vol. 35, pp. 3322-3332, 2010.
Tremblay 09	O. Tremblay, L.A. Dessaint, " Experimental Validation of a Battery Dynamic Model for EV Applications", Worl Electric Vehicul Journal, Vol 3, 2009.
Bird 81	R.E. Bird, R. L. Hulstrom, "Simplified Clear Sky Model for Direct and Diffuse Insolation on Horizontal Surfaces", Technical Report No. SERI/TR-642-761, Golden, CO: Solar Energy Research Institute, 1981.
Masters 13	G.M. Masters, "Renewable and Efficient Electric Power Systems, 2nd Edition", Wiley, IEEE Press, 2013.
Diagne 13	M. Diagne, M. David, P. Lauret, J. Boland, N. Schmutz, "Review of solar irradiance forecasting methods and a proposition for small-scale insular grids", Renewable and Sustainable Energy Reviews, Vol 27, pp. 65–76, 2013.
Perez 07	R. Perez, K. Moore, S. Wilcox, D. Renne, A. Zelenka, "Forecasting solar radiation – Preliminary evaluation of an approach based upon the national forecast database", Solar Energy, Vol 81, pp. 809-812,2007.
Pedro 12	H.T.C. Pedro, C. F.M. Coimbra," Assessment of forecasting techniques for solar power production with no exogenous inputs", Solar Energy, Vol 86, pp. 2017–2028, 2012.
Lora 02	C. Lora, J. Riquelme Santos, J. Riquelme Santos, A.G. Exposito, and J.L. Martınez Ramos, A Comparison of Two Techniques for Next-Day Electricity Price Forecasting, IDEAL 2002, LNCS 2412, pp. 384–390, 2002
Paoli 10	C.Paoli, C. Voyant, M. Muselli, M. Nivet," Forecasting of preprocessed daily solar radiation time series using neural networks", Solar Energy, Vol 84, pp. 2146–2160, 2010.

Shepherd 65 C.M. Shepherd, "Design of Primary and Secondary Cells - Part 2. An equation describing battery discharge", Journal of Electrochemical Society, Vol112, pp 657-664, 1965.

Martha 12 S.K. Martha, J. Nanda, G.M. Veith, N.J. Dudney, " Electrochemical and rate performance study of high-voltage lithium-rich composition: Li1.2Mn0.525Ni0.175Co0.1O2", Elsevier, Journal of Power Sources, Vol 199, pp 220–226, 2012.

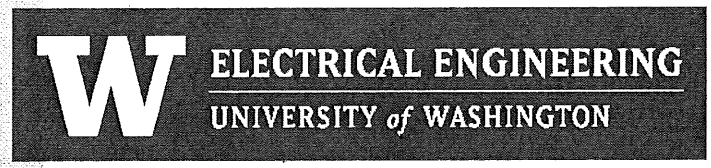

University of Washington
Department of Electrical Engineering
185 Stevens Way
Paul Allen Center - Room AE100R
Campus Box 352500
Seattle, WA 98195-2500